Experimental and Numerical Assessment on S-shaped Diffuser performance with different Turbulence Intensity

IOP Conf. Series: Materials Science and Engineering **765** (2020) 012046 doi:10.1088/1757-899X/765/1/012046

Experimental and Numerical Assessment on S-shaped Diffuser performance with different Turbulence Intensity

Raed Jessam[1]

Hussain H. Al-Kayiem[2]

Mohammad S. Nasif,[2]

Ameer Abed Jaddoa Albuali[1]

[1]Electromechanical Engineering Department, University of Technology, Baghdad, Iraq

[2]Mechanical Engineering Department, University of Technology, Petronas, Malaysia

corresponding author's e-mails : 50097@uotechnology.edu.iq, hussain_kayiem@utp.edu.my, mohammad.nasif@utp.edu.my

Abstract. The turbulence structure in air intake S-shaped diffuser is proven to be influencing parameter on the diffuser performance. In the present research work, experimental and numerical investigations have been undertaken to explore the effect of inlet turbulence intensity level on the performance of air intake S-shaped diffuser. Detailed measurements including pressure and velocity at the inlet and outlet planes and static pressure on the top and bottom walls were taken at three pre-selected Reynolds numbers of 4.8×104, 6.4×104 and 7.5×104. The predicted corresponding turbulence intensities at the experimented three Re, were 4.16%, 3.15% and 2.8%. ANSYS-FLUENT 15 software with Standard k-ε turbulence model has been used for numerical simulations. Numerical results of static pressure recovery, total pressure loss coefficient and wall static pressure recovery have been compared with the experimental results. The experimental results indicate that increasing Reynolds number at the inlet of S-shaped diffuser resulting in slight decrease in measured turbulence intensity. Also, as Re increased from 4.8x104 to 7.5x104, the static pressure recovery increased by 9% and the total pressure loss coefficient was reduced by 4.9%.

Keywords: distortion coefficient; CFD; S-shaped diffuser; turbulence intensity; static pressure coefficient.

Nomenclature

AR	area ratio ($AR=Ae/Ai$)	P_{ws}	wall static pressure (N/m^2)
Ae	cross section area of outlet plane	P_{wsi}	wall inlet static pressure (N/m^2)
Ai	cross section area of inlet plane	Re	Reynolds number
D_h	hydraulic diameter (mm)	P_t	total pressure (N/m^2)
C_{PR}	static pressure recovery coefficient	$P_{t\,ave\,o}$	outlet average total pressure (N/m^2)
C_{WPR}	wall static pressure coefficient	R_c	radius of curvature (mm)
C_{TL}	total pressure loss coefficient	U_{ave}	average velocity (m/s)
$T.I$	turbulence intensity	ρ	density of air (kg/m^3)
P_s	static pressure (N/m^2)	μ	viscosity of air (kg/m. s)
P_{si}	inlet static pressure (N/m^2)	AIP	aerodynamic inlet plane
P_{ti}	inlet total pressure (N/m^2)		

1. Introduction

The S-shaped diffuser is one of the widespread research topics in mechanical engineering due to the imperative applications for guiding flow at the aero-engine inlet, gas turbine inter-connecting-duct and engine exhaust. Therefore, S-shaped diffuser represented the main component of breathing aero-engines. The design of S-shaped diffusers is more complicated than regular diffusers since additional pressure losses are resulting from the complicated flow phenomena consisting of flow separation and circulating bubble, in high bending walls. The experimental and numerical investigation is complicated with the added challenges in predicting boundary layer growths and flow separation under the interactions between the secondary counter rotating flows and the adverse pressure gradient regions [1].

The main issue that is taken concern in the numerical simulation is the modeling of the turbulence. Wenbiao and Xiaocui [2] used SST turbulent model to get the optimum design of S-shaped diffuser. Xiao *et al*. [3] applied a modified *k*–ω turbulence model to investigate transonic flow features of an S-duct. Gerolymos *et al.* [4] adopted Reynolds Stress Model to analyze the flow field structure of a dual S-duct. Saha *et al*. [5] studied flow characteristics of the S-duct based on RNG *k*–ε turbulence model. Zhang *et al.* [6] used *k*–ε turbulence model to design an S-duct. Lee and Kim [7] were studied the sensitivity of the S-duct with different turbulence models. Zhang *et al.* [8] investigated multidisciplinary design strategy of an S-duct, which used SST *k*–ω turbulence model for numerical simulation. Gopaliya *et al*. [9-10] investigated S-shaped diffuser of 90^o/90^o turn with rectangular inlet (Aspect ratio = 2) and semicircular outlet (Aspect ratio = 2) by the effect of offset. The obtained show that the increase in Reynolds number (*Re*) leads to increase in coefficient of static pressure gain (C_{PR}).

Gavin *et al*. [11] investigated the Allison 250 gas turbine S-shaped diffuser. The calculated Allison 250 S-shaped diffuser flow features were then compared to those in a constant diameter S-shaped tube with the same inlet cross-sectional area and offset.

Gavin *et al*. [12] have investigated numerically six variations of the S-shaped diffuser geometry of the Allison 250 gas turbine with range of turbulence intensity (*T.I*) at one *Re* and with range of *Re* at one turbulence intensity. The qualitative results show that, the pressure coefficient variations for the three inlet *T.I* values considered are qualitatively similar. The quantitative results show that the highest inlet *T.I* returns slightly higher-pressure coefficients.

The present study focuses on the turbulent flow in the air intake S-shaped diffuser with different inlet *T.I* and different inlet *Re*. An experimental test rig is constructed and used to collect data that

have been used for validation. ANSYS-FLUENT15 with Standard k-ε turbulence model has been adopted as the investigation tool. The main performance parameters of S-shaped diffuser in terms of (C_{PR}), total pressure loss coefficient (C_{TL}) and wall static pressure coefficient (C_{WPR}) have been predicted to permit exploration of sensitivity of these parameters with the different inlet *T.I* and *Re*.

2. Experimental set up

The geometry of the S-shaped diffuser used in this study is shown in figure 1. It was designed based on area ratio *AR* of 3.1. The radius of curvature R_c = 280 mm, the turning angle θ = 45º. The total length of the diffuser L = 526 mm, and the hydraulic diameter D_h = 65 mm. The modeled diffuser has a constant area conduit at the inlet with 65 mm long x 65 mm height, for smooth air inflow, and constant area conduit at the outlet with 65 mm long x125 mm height.

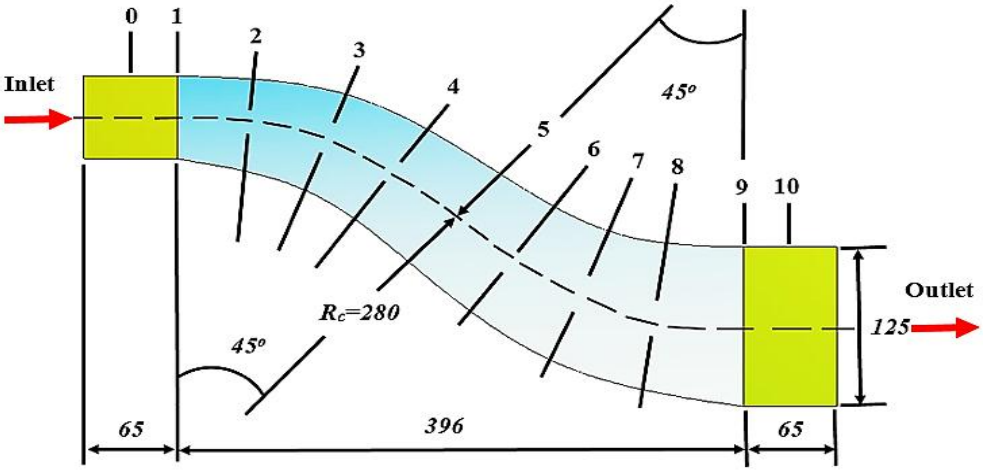

Figure 1: Geometry of the modeled S-shaped diffuser and plane of interest (all dimensions in mm)

An 1100 mm duct length which has same diameter of inlet S-shaped diffuser has been used to connect the air blowers with the S-shaped diffuser as shown in figure 2.

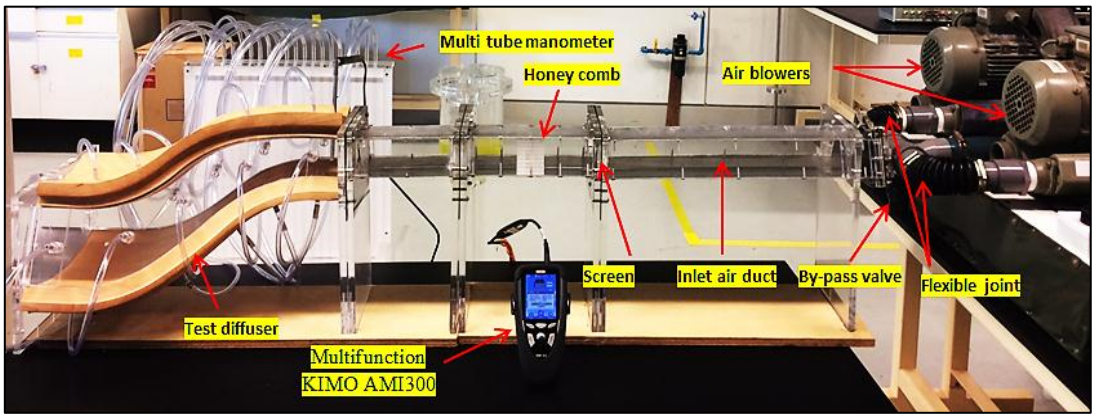

Figure 2: S-shaped diffuser Test Apparatus

Three inlet velocities have used for investigation 14.4 m/s,15.8m/s and 17.4 m/s, i.e three *Re* of 4.8×10^4, 6.4×10^4 and 7.5×10^4 obtained depending on the inlet hydraulic diameter of S-shaped diffuser. Also, it has been used for measuring the *T.I* experimentally at the inlet plane of S-shaped diffuser by interface the datalogger with PC as shown in figure 3. These inlet velocities and inlet turbulence intensities used an inlet boundary conditions for CFD simulation.

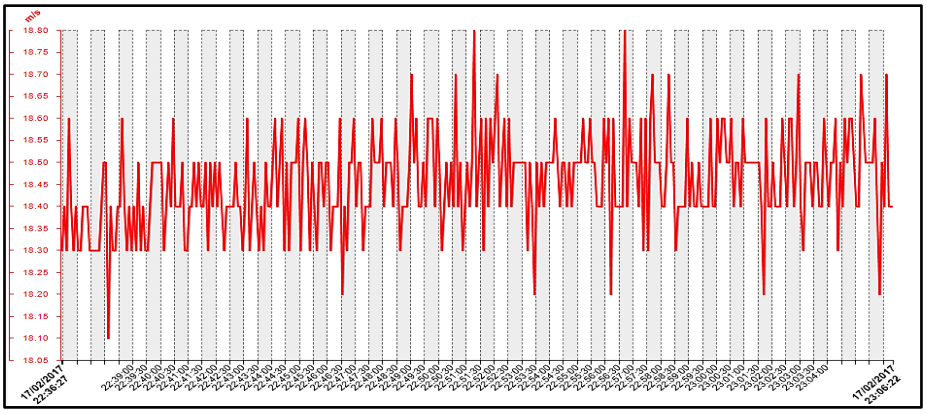

Figure 3: Measurement of *T.I* by velocity fluctuation with time at the inlet of S-shaped diffuser.

3. Performance parameters

The main important parameters are using for evaluation the performance of S-shaped diffuser in the current study are:

3.1. Wall static pressure coefficient CWPR

The wall static pressure coefficient is represented by the following equation:

$$C_{WPR} = \frac{P_{ws} - P_{wsi}}{\frac{1}{2}\rho U_{ave\,i}^2} \quad (1)$$

3.2. Static pressure recovery coefficient CPR

It represents the magnitude by which kinetic energy has been converted into pressure energy due to diffusing action at any location along the S-shaped diffuser, it is represented by the equation:

$$C_{PR} = \frac{P_s - P_{si}}{\frac{1}{2}\rho U_{avi}^2} \quad (2)$$

3.3. Total pressure loss coefficient CTL

It is a measure of how much total pressure is lost as a proportion of the mean inlet dynamic pressure due to viscous forces and turbulent mixing, this defined by the equation

$$C_{TL} = \frac{P_{ti} - P_t}{\frac{1}{2}\rho U_{avi}^2} \quad (3)$$

4. Numerical Approach

4.1. Mesh generation

The S-shaped diffuser used in the experiments was modeled by modular design ANSYS 15 for CFD simulation, a mesh generation by ANSYS - FLUENT 15. Figure 4 shows the unstructured mesh along the S-shaped diffuser.

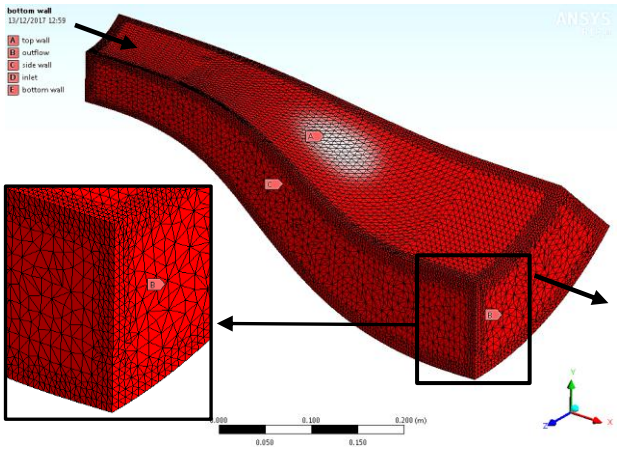

Figure 4: Unstructured mesh of S-shaped diffuser

4.2. Mesh independency checking

When doing analysis of any CFD problem using software or code the first important and necessary thing is checking the mesh dependency, because of the solution has a great dependency on the fineness of meshing. In this study, Different meshes have been checked for S-shaped diffuser for $Re = 6.4\times10^4$ and $T.I = 3.15$, with performance parameter C_{WPR} on the top and bottom walls as shown in figure 5-A and 5-B, respectively.

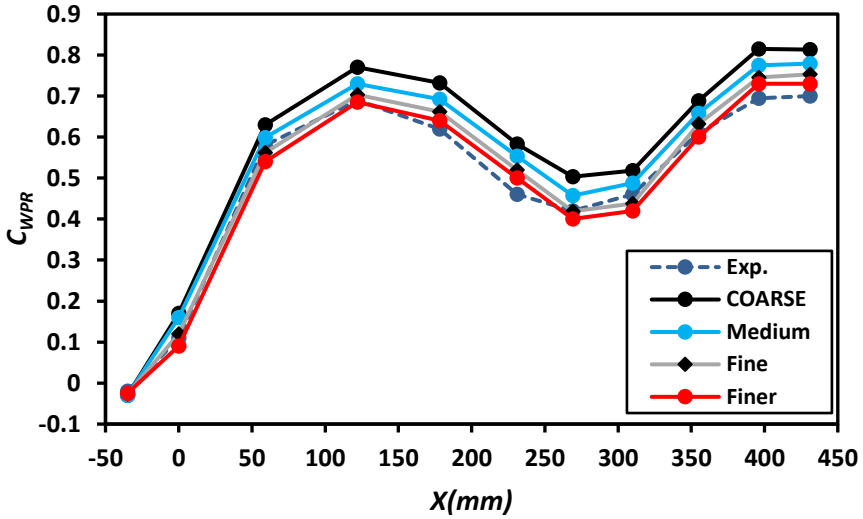

A. Top wall

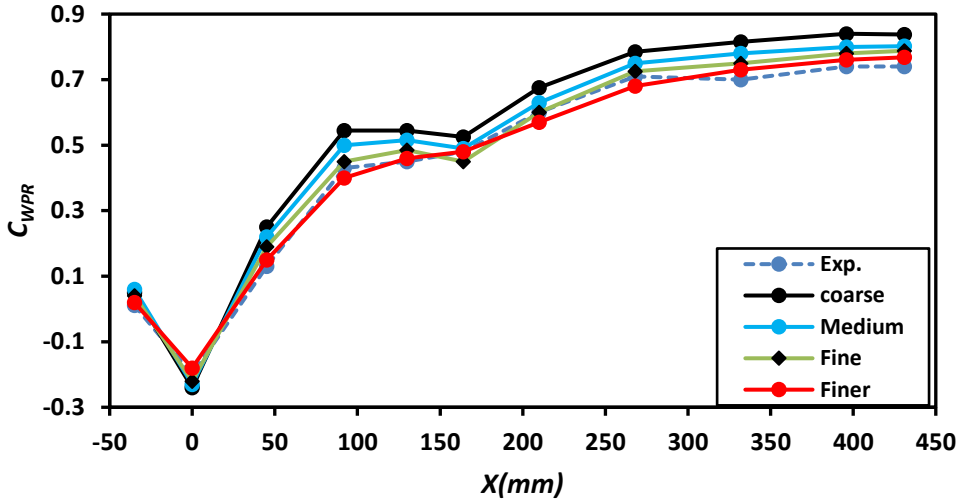

B. Bottom wall

Figure 5: Calculated C_{WPR} with different grid resolution: A. top wall, B. bottom wall

Refining the mesh from coarse to medium, results in a significant change of the C_{WPR} values as much as 11% at the top wall and 12% at the bottom wall. A further refinement of the mesh results in an average variation of the C_{WPR} values of 5.5% and 7% at the top and bottom walls, respectively. This variation drops to 1.4% at the top wall and 2.6% bottom wall when fine mesh is compared to the finer mesh which has 119548 volume cells. This means that with fine mesh results were almost independent of the computational mesh, and the mesh could be used with certainty for validation. The important features of these meshes are summarized in table 1.

Table 1. Grid independency check.

Mesh No.	No. of volume cells	C_{WPR} of top wall		C_{WPR} of bottom wall	
		CFD	Error %	CFD	Error %
coarse	19404	0.81	11	0.84	12
medium	82042	0.77	5.5	0.80	7
fine	119548	0.74	1.4	0.77	2.6
finer	124572	0.73	-	0.75	-

4.3. Boundary conditions

For the CFD simulations of S-shaped diffuser, same values of inlet velocity profile and *T.I* as found experimentally are used as input for velocity inlet and *T.I* boundary conditions.. Enhanced wall treatment was adopted for near wall treatment. No slip boundary condition was specified at the walls of S-shaped diffuser. Finally, all simulation cases were performed with standard air properties at the temperature 30^{o}C, as below:
Inlet Reynolds number: (4.8×10^{4}, $6.4\times10^{4,}$ 7.5×10^{4})
Inlet Turbulence intensity: (4.16 %, 3.15 %, 2.8 %)
Outlet gauge pressure: (0 Pa)
Air density: (1.1649 kg/m^{3})
Air viscosity: (1.868×10^{-5} kg/ (m s))

4.4. Governing equations

The governing equations for continuity and momentum, three–dimensional, steady state, Reynolds Average Navier Stokes (RANS) equations were numerically solved turbulent incompressible flows of air [13]. The 3D Standard *k–ε* model for simulating the turbulence quantities has been adopted. The enhanced wall treatment was opted to cope with high complex three-dimensional near wall flow phenomena of diffusers. The inlet boundary conditions were selected like those of the experimental inlet conditions. Near-wall modeling is performed with enhanced wall treatment method to address the boundary layer formed during grid generation.

4.5. Validation

The calculated C_{WPR} using the *Re* of 6.4×10^{4} and *T.I* of 3.15% at the inlet of the S-shaped diffuser, and the ANSYS-FLUENT Standard *k-ε*, RNG *k-ε* and Realizable *k-ε* turbulence models are compared with the experimental data in figure 6. Very good quantitative and qualitative agreement can be observed between the experimental data and Standard *k-ε* turbulence model data along the length of S-shaped diffuser. An observation of the validation results from table 2 the predicted results by Standard *k-ε* model was better agreement with the experimental results compared to the RNG *k-ε* and Realizable *k-ε* turbulence models. The Standard *k-ε* model predicts C_{WPR} as 0.73 and 0.75 on the top and bottom wall, respectively, which is closer to the experimental results of 0.69 and 0.74. This is correspondent to NG & Birk (2013) [1] and Gopaliya *et al*. [10].

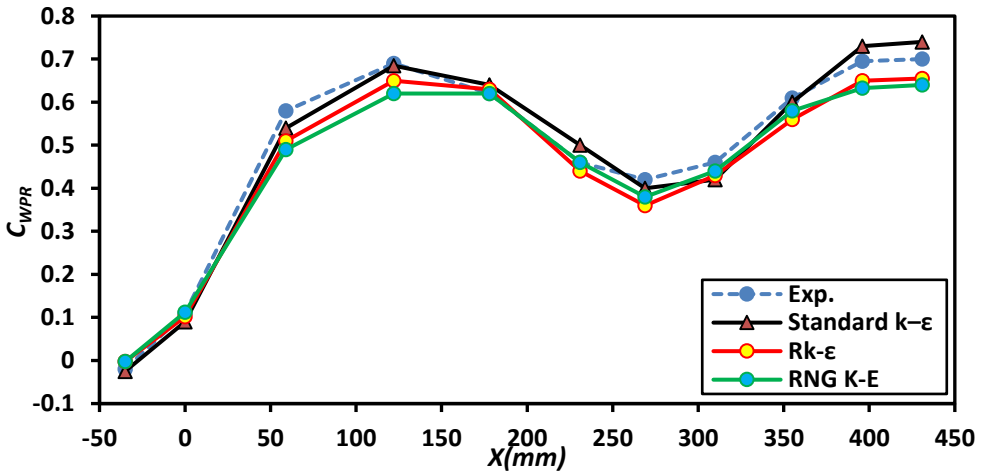

(A)

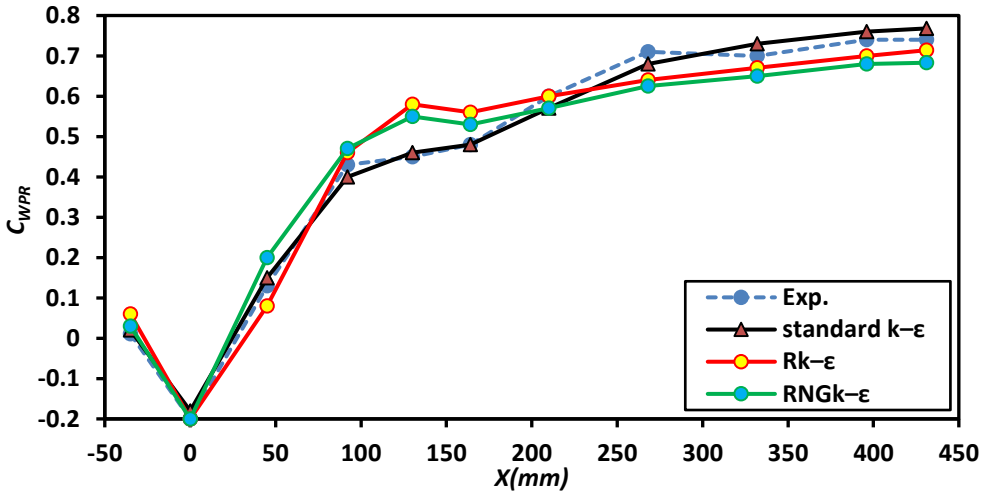

(B)

Figure 6: Comparison of experimental values of C_{WPR} with different turbulence models: A. Top surface, B. Bottom surface.

Table 2: Comparison of C_{PR} values of experimental study with values of CFD turbulence models

Type of study	Top wall		Bottom wall	
	C_{WPR} value	Deviation %	C_{WPR} value	Deviation %
CFD- R *k-ε*	0.65	5.8	0.7	5.4
CFD- RNG *k-ε*	0.63	8.7	0.68	10.8
CFD- Stand. *k– ε*	0.73	5.8	0.75	2.5
Experimental	0.69	-	0.74	-

5. Results and discussion

5.1. Flow field structure in the S-shaped Diffuser

The development of flow velocity along the S-shaped diffuser at Re = 6.4×10^4 and $T.I.$ = 3.15 is showing in figure 7. After the inlet plane, the longitudinal velocity profile trend to distort towards the bottom surface due to the concave shape of bottom wall of diffuser in addition to high curvature at the first bend. While the flow near the top surface is decelerated until the first bend at X=120 mm approximately. After the first bend, the flow will be accelerating with the top wall and decelerate with bottom wall until the outlet plane after the second bend. This behavior of flow due to the secondary flow which is resulting from increase flow separation zone at the bottom surface.

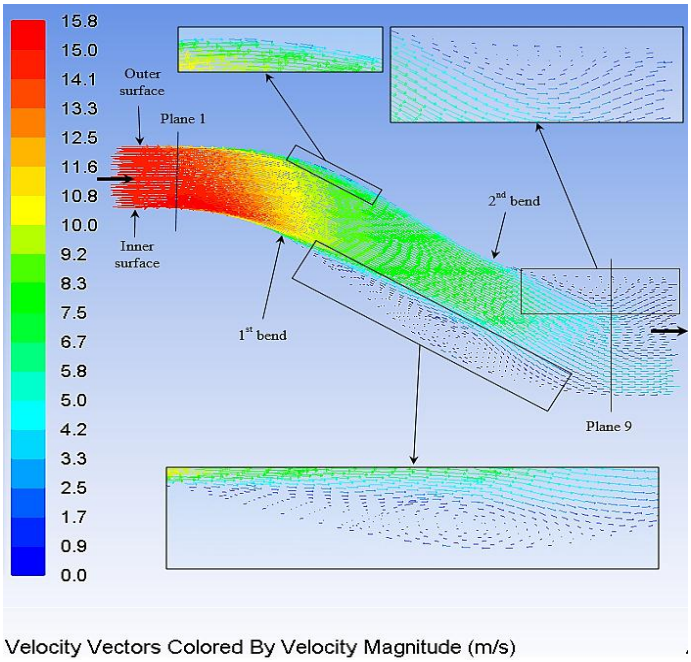

Figure 7: Development of the flow field structure in the S-shaped Diffuser by velocity vectors

Figure 8 describe the development of flow velocity by velocity vectors on the top and bottom walls at Re = 6.4×10^4 and T. I = 3.15%. The flow velocity decreased on the top wall until the first bend at X = 120mm, after that the flow velocity increased until the second bend at X = 270mm and then decreased in the direction of outlet due to the increase of cross-sectional area and back flow as illustrated in figure 8-A. On the bottom wall of S-shaped diffuser the flow on the first bend undergoes a larger acceleration and hence diffusion due to the high bending of wall, as shown in figure 8.B. This part of the flow was found to be responsible for a significant part of the overall duct total pressure loss caused by a flow separation zone at the bottom surface.

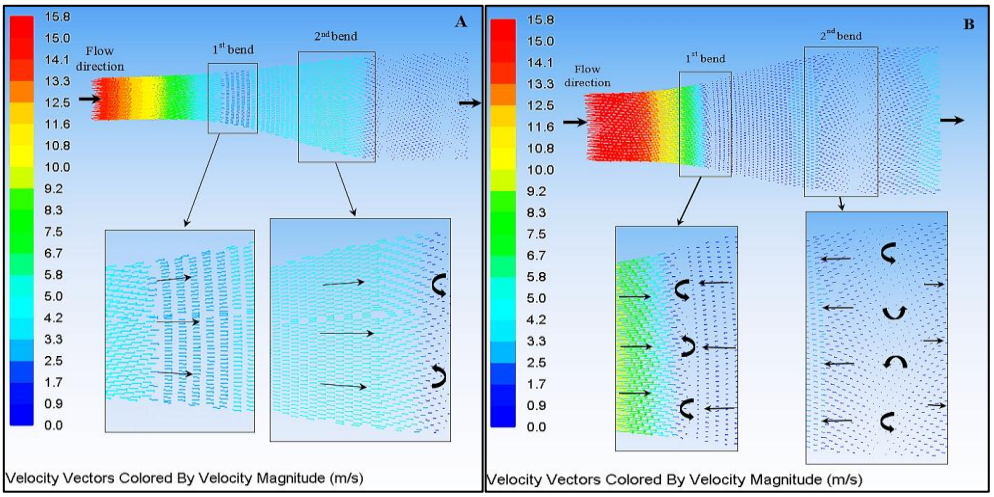

Figure 8. S-shaped diffuser with development of velocity vector at Re 1 = 6.4×104 and T. I1 = 3.15% on the: A. top wall (top view), B. bottom wall (top view).

5.2. Wall Static Pressure Recovery CWPR

The C_{WPR} is one of the performance parameters which can be determined by measuring wall static pressure on the top and bottom walls along the length of S-shaped diffuser. figure 9 presents the distribution of C_{WPR} on the top wall for S-shaped diffuser. The trend of C_{WPR} for experimental and CFD results is similar by recovering until the first bend. The maximum value of C_{WPR} from experimental and CFD investigation at the first bend is 0.75 and 0.62, respectively at $X \approx 150$ mm with *Re* 3. After that, the C_{WPR} dropped to be around 0.38 and 0.42 for experimental and CFD results, respectively at $X \approx 270$mm. This drop resulting from the accelerating flow between the first and second bend due to high curvature. The flow separation zone indicated at the second bend at $X \approx$ (240 -320) mm for S-shaped diffuser. After the second bend, the C_{WPR} is recovering to the outlet plane for both diffusers due to the decelerating flow resulting from expansion cross sectional area.

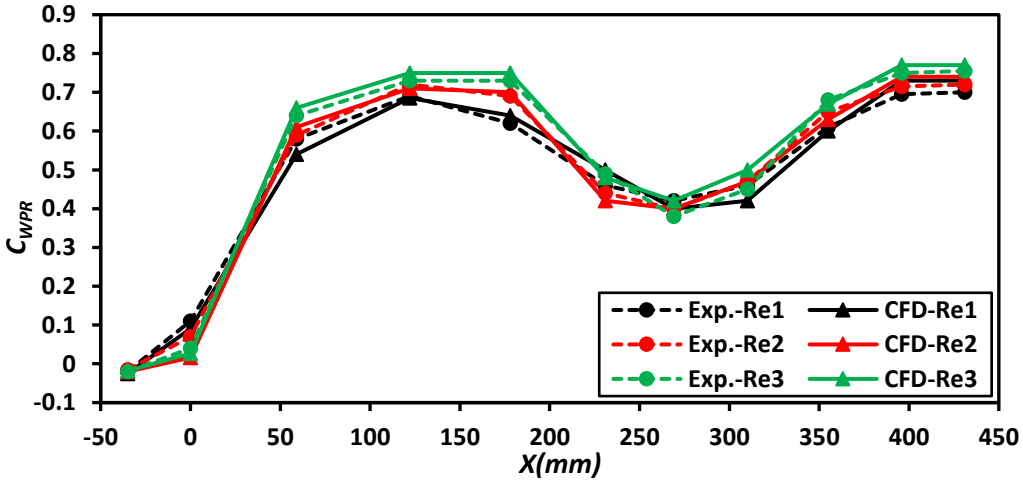

Figure 9: Distribution of CWPR along the top wall with, Re 1 = 5.8×104, T. I1 = 4.16%, Re 2 = 6.4×104, T. I2= 3.15%, Re 3= 7.5×104, T. I3= 2.8%

The trend of C_{WPR} along the bottom wall showed a continuous increase after an initial decrease at the start of the first bend as shown in figure 10. This initial decrease was observed by other researchers Sullerey *et al*. [14] and Asghar *et al*. [15]. This drop in C_{WPR} indicates an acceleration of the flow, while the rise in static pressure signifies a strong adverse pressure gradient. During the first bend, the bottom surface of the diffuser is the region where low momentum fluid exists. The C_{WPR} value after this drop increased due to high diffusion resulting from the expansion of cross-sectional area of S-shaped diffuser and may be due to the formed separation bubble as indicated approximately between X =90mm-160 mm.

Generally, the behavior of C_{WPR} at the bottom wall has an opposite trend to that of the top wall. The increase of Re from 4.8×10^4 to 7.5×10^4 leading to increase C_{WPR} on the top wall from 0.69 to 0.75 and from 0.73 to 0.77 for the experimental and CFD investigation, respectively. While the C_{WPR} was increase on the bottom wall from 0.74 to 0.81and from 0.76 to 0.83 for experimental and CFD investigation. In addition, the experimental results were lower in both top and bottom walls as compared to the CFD results and there is a deviation between the experimental and CFD results may be due to surfaces finish where in the experiments the S-shaped diffusers were made using wood be different from the surface finish assumed in the CFD simulations.

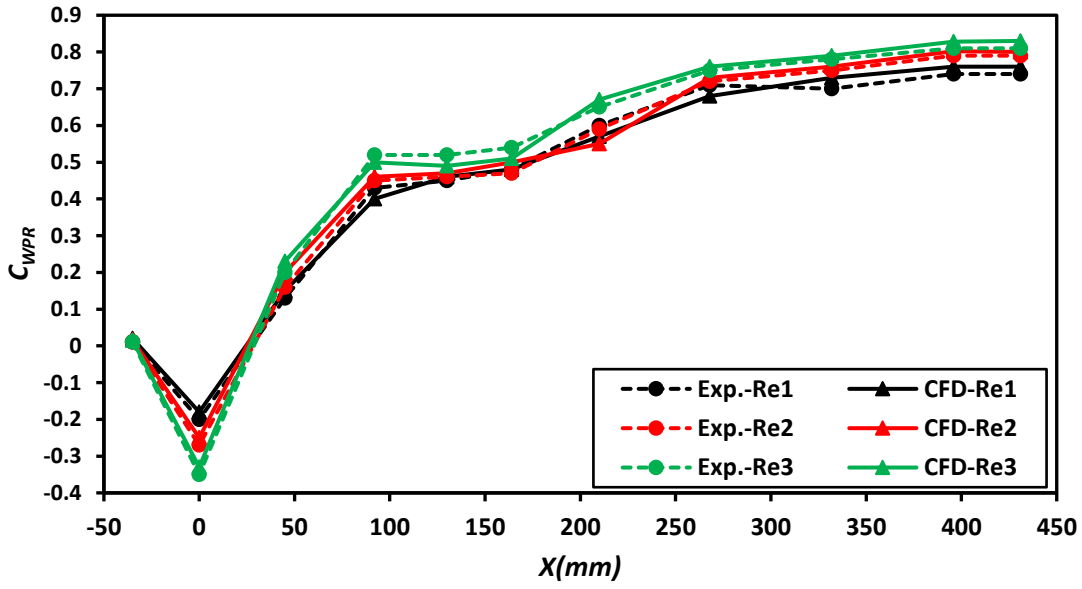

Figure 10: Distribution of CWPR along the bottom wall with, Re 1 = 5.8×104, T. I1 = 4.16%, Re 2 = 6.4×104, T. I2= 3.15%, Re 3= 7.5×104, T. I3= 2.8%

5.3. Static Pressure Recovery CPR

Figure 11 shows the variation of static pressure recovery coefficient C_{PR} along the length of the S-shaped diffuser. C_{PR} is computed, experimentally by test rig measurements and numerically with CFD, with different Re and $T.I$. The C_{PR} values computed by CFD at $Re = 4.8\times10^4$ increase in the initial phase up to plane 3 around $X \approx 120$mm is observed. After that it drops due to flow separation until flow reattachment occurs somewhere before plane 7 at $X \approx 240$mm and then it increases steadily till the exit plane. At the same case with experimental measurements the trend of C_{PR} similar to the C_{PR} by

CFD with some deviations in the location or length of the separated flow region. C_{PR} increase in the initial phase up to around $X \approx 100$mm and then it decreases due to flow separation. The flow separation occurs early with experimental measurements and flow reattachment occurs at $X \approx 205$mm. This trend of C_{PR} can be observed with the $Re = 6.4\times10^4$ and $Re = 7\times10^4$, for the experimental and numerical investigations.

In general, the C_{PR} increases with increasing from Re_1=4.8×10^4 to Re_3= 7.5×10^4 from 0.71 to 0.78 and from 0.75 to 0.8 for experimental and numerical investigation. This improvement of C_{PR} may be resulting from increase the mixing level between the core flow of high kinetic energy with the flow of low kinetic energy close to the bottom wall.

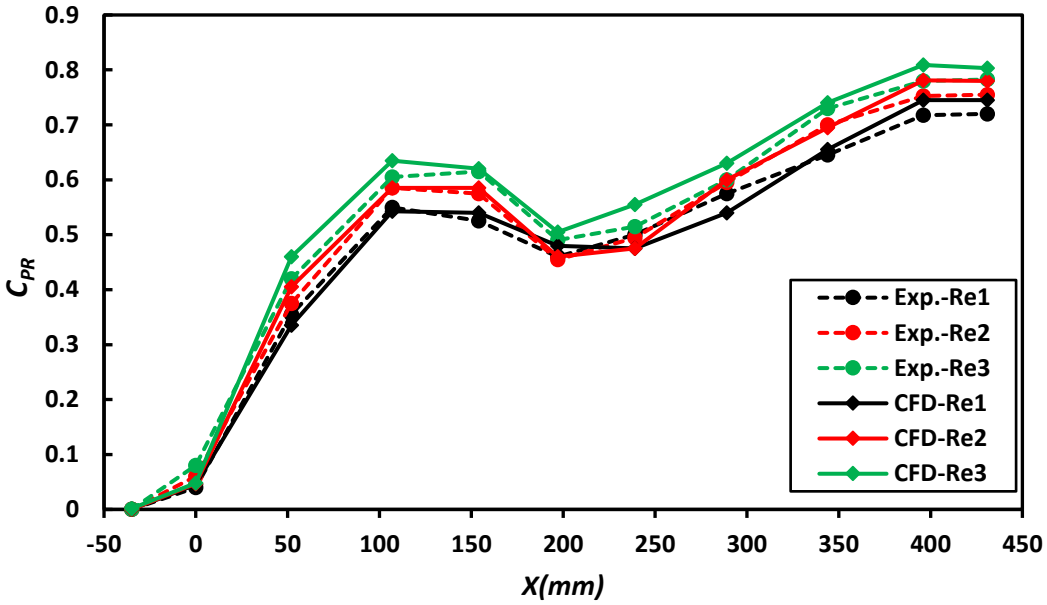

Figure 11: Comparison of experimental and numerical results of CPR along the length of S-shaped diffuser for various Re.

5.4. Total pressure loss coefficient, CTL

Figure 12 shows that the C_{TL} decreases with increase the Re along the centerline length of S-shaped diffuser. The experimental results of C_{TL} reduced from 0.28 to 0.263 and the CFD results reduced from 0.257 to 0.245 as illustrated in Fig. 12. This reduction be due to the reduction of flow separation zone which is resulting from increase the mixing level between the flow of high kinetic energy with the flow of low kinetic energy close to the bottom wall as mentioned previously.

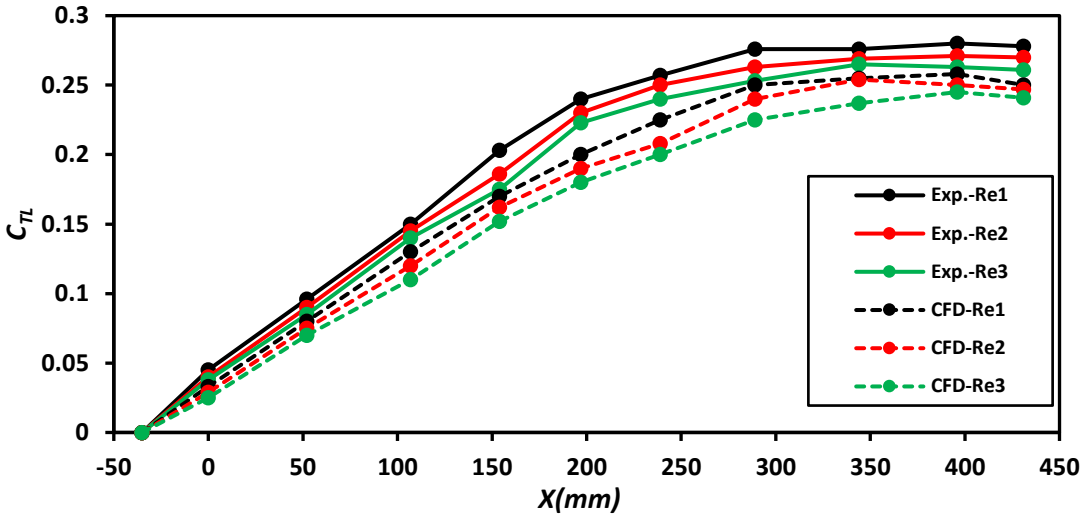

Figure 12. Comparison of Experimental and numerical results of CTL along the length of S-shaped diffuser for various Re.

There is a deviation between the experimental results and the CFD results of C_{TL} with the investigated range of *Re*, the higher value of 7.6% with Re_2 and the lower value of 6% with Re_1, as in Table 3. This deviation may be due to the small fluctuation of inflow during the experimental test compared to constant inflow assumed with CFD simulation, thereby the values of C_{TL} are affected by the inflow conditions.

Table 3. Experimental and numerical results of CTL along the length of S-shaped diffuser.

Re	C_{TL} value		
	Experimental	CFD	Deviation%
4.8×10^4	0.28	0.257	6
6.4×10^4	0.271	0.25	7.6
7.5×10^4	0.263	0.245	6.8

6. Conclusions

Experimental and numerical studies have been conducted on S-shaped diffuser with range of *Re* from 4.8×10^4 to 7.5×10^4. The following conclusions have been drawn from current investigations:

- Increase *Re* from 4.8×10^4 to 6.4×10^4 and 7.5×10^4 experimentally resulting in slightly reduction in the measured inlet *T.I* as, 4.16%, 3.15% and 2.8%, respectively.
- Increase in *Re* from 5.8×10^4 to 7×10^4 resulting in increase in the wall static pressure recovery, C_{WPR} for both top and bottom walls, as demonstrated by the experimental and numerical results.
- Increase in *Re* 4.8×10^4 to 7.5×10^4 resulting in increase in static pressure recovery coefficient for both CFD results from 0.75 to 0.8 (6.2%) and experimental results from 0.71 to 0.78 (9%), respectively. Also, a difference has been realized between the experimental and the CFD

pressure recovery coefficient results around 5.6%, 4% and 2.5% at 4.8×10^4 to 6.4×10^4 and 7.5×10^4 Reynolds numbers, respectively

- The total pressure loss coefficient C_{TL} is decreasing from 0.28 to 0.263(6.4) for CFD results and from 0.257 to 0.245(4.9) for experimental results as *Re* values increasing from 5.8×10^4 to 7×10^4.

References

[1] Ng, B. C., & Birk, A. M. (2013, June). Experimental and CFD Study of a Rectangular S-Bend Passage with and Without Pressure Recovery Effects. In ASME Turbo Expo 2013: Turbine Technical Conference and Exposition (pp. V06BT38A008-V06BT38A008). American Society of Mechanical Engineers

[2] Gan, W., & Zhang, X. (2016). Design optimization of a three-dimensional diffusing S-duct using a modified SST turbulent model. Aerospace Science and Technology.

[3] Xiao, Q., Tsai, H. M., & Liu, F. (2003). Computation of Transonic Diffuser Flows by a Lagged k-? Turbulence Model. Journal of propulsion and power,19(3), 473-483.

[4] Gerolymos, G. A., Joly, S., Mallet, M., & Vallet, I. (2010). Reynolds-stress model flow prediction in aircraft-engine intake double-S-shaped duct. Journal of Aircraft, 47(4), 1368-1381.

[5] Saha, K., Singh, S. N., Seshadri, V., & Mukhopadhyay, S. (2007). Computational analysis on flow through transition s-diffusers: effect of inlet shape. Journal of aircraft, 44(1), 187-193.

[6] Zhang, W. L., Knight, D. D., & Smith, D. (2000). Automated design of a three-dimensional subsonic diffuser. Journal of Propulsion and Power, 16(6), 1132-1140.

[7] Lee, B. J., & Kim, C. (2007). Automated design methodology of turbulent internal flow using discrete adjoint formulation. Aerospace Science and Technology, 11(2-3), 163-173.

[8] Zhang, J. M., Wang, C. F., & Lum, K. Y. (2008). Multidisciplinary design of S-shaped intake. In 26th AIAA Applied Aerodynamics Conference (p. 7060).

[9] Gopaliya, M. K., Kumar, M., Kumar, S., & Gopaliya, S. M. (2007). Analysis of performance characteristics of S-shaped diffuser with offset. Aerospace Science and Technology, 11(2-3), 130-135.

[10] Gopaliya, M. K., Goel, P., Prashar, S., & Dutt, A. (2011). CFD analysis of performance characteristics of S-shaped diffusers with combined horizontal and vertical offsets. Computers & fluids, 40(1), 280-290.

[11] Lee, G. G. W., Allan, W. D. E., & Boulama, K. G. (2012, June). Numerical and experimental analysis of the airflow inside an A250 diffuser tube. In ASME Turbo Expo 2012: Turbine Technical Conference and Exposition (pp. 1703-1712). American Society of Mechanical Engineers.

[12] Lee, G. G., Allan, W. D., & Boulama, K. G. (2013). Flow and performance characteristics of an Allison 250 gas turbine S-shaped diffuser: Effects of geometry variations. International Journal of Heat and Fluid Flow, 42, 151-163.

[13] Ahmed.K. A., "Turbulence Modelling "in Introduction to Computational Fluid Dynamics(CFD)2008: USM, 2008.

[14] Sullerey, R. K., Chandra, B., & Muralidhar, V. (1983). Performance comparison of straight and curved diffusers. Defence Science Journal, 33(3), 195-203.

[15] Asghar, A., Stowe, R.A., Allan, W.D. and Alexander, D., 2017. Entrance Aspect Ratio Effect on S-Duct Inlet Performance at High-Subsonic Flow. Journal of Engineering for Gas Turbines and Power, 139(5), p.052602.